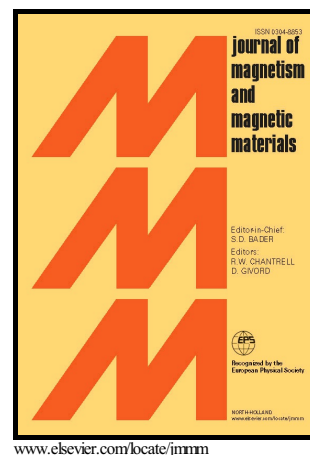


Author's Accepted Manuscript

A new type of magnetocaloric composite based on
conductive polymer and magnetocaloric compound

W. Imamura, A.A. Coelho, V.L. Kupfer, A.M.G.
Carvalho, J.G. Zago, A.W. Rinaldi, S.L. Favaro,
C.S. Alves



PII: S0304-8853(16)31417-2
DOI: <http://dx.doi.org/10.1016/j.jmmm.2016.10.120>
Reference: MAGMA62033

To appear in: *Journal of Magnetism and Magnetic Materials*

Received date: 12 July 2016
Revised date: 15 September 2016
Accepted date: 17 October 2016

Cite this article as: W. Imamura, A.A. Coelho, V.L. Kupfer, A.M.G. Carvalho, J.G. Zago, A.W. Rinaldi, S.L. Favaro and C.S. Alves, A new type of magnetocaloric composite based on conductive polymer and magnetocaloric compound, *Journal of Magnetism and Magnetic Materials* <http://dx.doi.org/10.1016/j.jmmm.2016.10.120>

This is a PDF file of an unedited manuscript that has been accepted for publication. As a service to our customers we are providing this early version of the manuscript. The manuscript will undergo copyediting, typesetting, and review of the resulting galley proof before it is published in its final citable form. Please note that during the production process errors may be discovered which could affect the content, and all legal disclaimers that apply to the journal pertain.

A new type of magnetocaloric composite based on conductive polymer and magnetocaloric compound

W. Imamura^{a*}, A.A. Coelho^b, V.L. Kupfer^c, A.M.G. Carvalho^d, J.G. Zago^a, A.W. Rinaldi^c, S.L. Favaro^a, C.S. Alves^a

^a State University of Maringá (UEM)/Department of Mechanical Engineering (DEM-PEM), 87020-900, Maringá, PR, Brazil

^b State University of Campinas (Unicamp)/Department of Applied Physics (DFA-IFGW), 13083-859, Campinas, SP, Brazil

^c State University of Maringá (UEM)/Department of Chemistry (DQI-LMSen), 87020-900, Maringá, PR, Brazil

^d Brazilian Synchrotron Light Laboratory (LNLS)/Brazilian Center for Research in Energy and Materials (CNPEM), C. P. 6192, 13083-970, Campinas, SP, Brazil

* Corresponding author. williamimamura@yahoo.com.br (W. Imamura)

Abstract

We introduce a processing route of the first magnetocaloric composite with conductive polymer – wherein the magnetocaloric reinforcement is a compound $\text{Gd}_{5.09}\text{Ge}_{2.03}\text{Si}_{1.88}$ and the ductile matrix is a conductive polymer polyaniline doped by camphorsulfonic acid (PAni-CSA). This new type of composite combines mechanical, electrical and magnetocaloric properties that can be applied in thermomagnetic machines.

Keywords

magnetocaloric effect; magnetocaloric properties; magnetic properties; magnetic refrigeration.

1. Introduction

Magnetocaloric materials can be applicable in magnetic cooling technologies, thermomagnetic motors or medical treatments [1,2]. Since Pecharsky and Gschneidner Jr. [3] discovered the giant magnetocaloric effect (GMCE) in $\text{Gd}_5\text{Ge}_2\text{Si}_2$ compound, several studies – such as heat-treatments [4], effect of impurities [5], hydrogenation [6], cooling rate [7], pressure-induced effects [8] and particle size [9] – were done to investigate how the magnetic and magnetocaloric properties could be changed and how these could be related to phases and compositions.

Gama *et al.* [10] showed that samples of $\text{Gd}_5\text{Ge}_2\text{Si}_2$ is not strictly stoichiometric, but it is $\text{Gd}_{5.09}\text{Ge}_{2.03}\text{Si}_{1.88}$. Furthermore, Pires *et al.* [11] observed that $\text{Gd}_{5.09}\text{Ge}_{2.03}\text{Si}_{1.88}$ as-cast compound undergoes a first- and second-order transition; in other words, $\text{Gd}_{5.09}\text{Ge}_{2.03}\text{Si}_{1.88}$ as-cast compound exhibits GMCE without heat-treatment.

However, to glimpse some applicability of $\text{Gd}_{5.09}\text{Ge}_{2.03}\text{Si}_{1.88}$ as-cast compound, it is necessary to regard processes after the melting process because in almost cases the magnetocaloric material will need a specific geometry (*e.g.*, plates, cylinders, spheres, nanoparticles, etc.), but $\text{Gd}_{5.09}\text{Ge}_{2.03}\text{Si}_{1.88}$ is fragile.

Previous works with other fragile magnetocaloric materials resort to epoxy resins [12,13,14,15], which reduce the performance when applied to magnetic refrigeration. Besides, these works do not show mechanical properties about these magnetocaloric composites. On other hands, Lanzarini *et al.* [16] show mechanical properties about La-Fe-Si composites obtained by injection or extrusion moulding, but they not show any magnetocaloric properties and resort to polypropylene, that is an insulating thermoplastic polymer.

In light of this, the present study propose a new type of magnetocaloric composite with a matrix based on conductive polymer, PANi-CSA, and $\text{Gd}_{5.09}\text{Ge}_{2.03}\text{Si}_{1.88}$ as magnetocaloric reinforcement. This new processing route eliminates epoxy resins and thermoplastics

polymers; in other words, we aim to increase the thermal exchange, because this condition is fundamental for better efficiency in cooling technologies.

2. Experimental

2.1. Magnetocaloric reinforcement: $Gd_{5.09}Ge_{2.03}Si_{1.88}$

The purity of the starting elements Gd, Ge and Si are 99.9, 99.999 and 99.95 wt.%, respectively. The $Gd_{5.09}Ge_{2.03}Si_{1.88}$ as-cast compound was prepared by arc melting under inert argon atmosphere, and homogenized by turning the bulk for re-melting more two times. The cooling was rapidly performed in a water-cooled copper hearth. In total, we made 21 bulk samples with ~5 g, and the loss weight of each bulk was <2 wt.%. For the magnetocaloric composite confection, the 21 bulk samples were manually milled and mixed to obtain a homogeneous base-powder, then separated into particle size of 38-45 μm .

We analyzed the geometry of the magnetocaloric reinforcement $Gd_{5.09}Ge_{2.03}Si_{1.88}$ by scanning electron microscope (SEM). X-ray diffraction (XRD) was performed at the XRD1 beamline at Brazilian Synchrotron Light Laboratory (LNLS) [17]. Magnetic measurements were performed in a commercial magnetometer (MPMS, from Quantum Design) equipped with a superconducting quantum interference device (SQUID).

The magnetization (M vs. T) curves were measured with fixed magnetic fields at 200 Oe, increasing the temperature at the rate of 2 K/min, from 220 to 330 K, and decreasing at 2 K/min, from 330 to 220 K. From a simple numeric differentiation of the magnetization data, we calculated the temperature of first- and second-order transitions by a local minimum at dM/dT vs. T curves. The isothermal magnetization (M vs. H) curves were measured increasing the magnetic field with steps of 2 kOe up from 0 to 20 kOe and isotherms with steps of 2 K up from 250 to 300 K. From the isothermal magnetization data, we calculated the isothermal variation of the entropy (ΔS_T) by the numeric approximation,

$$\Delta S_T(T_{av})_{\Delta H} = \frac{\delta H}{2\delta T} \left(\delta M_1 + 2 \sum_{k=2}^{n-1} \delta M_k + \delta M_n \right) \quad (1)$$

proposed by Pecharsky and Gschneidner Jr. [18], where T_{av} is the average temperature between two consecutive isotherms (T_u and T_l), δT is the temperature steps, δH is the magnetic field step, and δM is the difference between magnetization at T_u and T_l for each magnetic field step from 1 to n .

From isothermal variation of entropy ($-\Delta S_T$ vs. T) curves, we also calculated the relative cooling power (RCP),

$$RCP(S) = |-\Delta S_T^{pk}| \times \delta T_{FWHM} \quad (2)$$

where $-\Delta S_T^{pk}$ is the magnitude of the peak, and δT_{FWHM} is the range of temperature at its full width at half maximum [19].

2.2. Conductive polymer: PANi-CSA

Aniline monomer (99.0 wt.%) was bidistilled to remove photooxidation's products (*e.g.*, water and ethanol). The oxidative polymerization was based on 1:1:1 reaction. Fresh aniline was dissolved in the dopant camphorsulfonic acid – CSA (0.1 mol.L⁻¹ of CSA) and ammonium persulfate – APS (0.05 mol.L⁻¹ of APS) added dropwise into the solution with constant mechanical stirring at a reaction temperature of 265 K. The reaction mixture was stirred for an additional 24 h at 265 K and then the product was filtered and rinsed with distilled water and methanol. The green powder of polyaniline doped by camphorsulfonic acid (PANi-CSA) obtained was dried at 343 K for 12 h and powdered to guarantee a refined material.

We used XRD (Cu-K α radiation, current of 30 mA, potential 30 kV, 2°/min, 2 θ from 5 to 80°), thermogravimetry–TG (heating rate of 10 K/min, from 298 to 1273 K, under N₂ flux of 50 mL/min), differential scanning calorimetry–DSC (heating rate of 10 K/min, from 298 to

623 K, under N₂ flux of 50 mL/min), Fourier transform infrared spectroscopy–FTIR (from 400 a 1800 cm⁻¹, step of 0,5 cm⁻¹), ultraviolet-visible spectroscopy–UV-Vis (PAni-CSA in 0.1 g.L⁻¹ of dimethyl sulfoxide, from 200 to 800 nm) and electrochemical impedance spectroscopy–EIS (triplicate, from 10 mHz to 100 kHz with potential fixed at 100 mV, according to ref. [20]) to characterize our PAni-CSA.

2.3. Magnetocaloric composite: PAni-CSA/Gd_{5.09}Ge_{2.03}Si_{1.88}

We made 6 samples of PAni-CSA/Gd_{5.09}Ge_{2.03}Si_{1.88} in duplicates (Table 1) varying two factors: Factor A – concentration of PAni-CSA (numerical type, wt.%); and Factor B – sintering at 443 K for 5 h (categorical type, sintering and non-sintering). All PAni-CSA/Gd_{5.09}Ge_{2.03}Si_{1.88} samples had 0.200 g, and was made mixing PAni-CSA and Gd_{5.09}Ge_{2.03}Si_{1.88} powder with gran size of 38-45 µm, than manually compacted in a steel matrix (Ø = 5 mm) at 250 MPa for 90 s followed by a load relief for 30 s, and again applied load at 250 MPa for 90 s. In the case of sintered samples, the sintering process was made under inert argon atmosphere by ramps and landings scheme: (a) heating rate of 5 K/min from room temperature to 373 K; (b) 30 min at 373 K to eliminate humidity; (c) heating rate of 5 K/min from 373 to 443 K; (d) 5 h at 443 K; and (e) natural cooling from 443 K to room temperature.

The mechanical properties PAni-CSA/Gd_{5.09}Ge_{2.03}Si_{1.88} composites were analyzed by Vickers hardness test method at bottom and top of the pallets, with microindentation of 300 g for 30 s. The pallets were fractured for SEM images. The magnetic measurements were performed via SQUID as described in section 2.1.

3. Results and discussion

3.1. $Gd_{5.09}Ge_{2.03}Si_{1.88}$

From a qualitative analysis from XRD (Fig. 1), the $Gd_{5.09}Ge_{2.03}Si_{1.88}$ compound with particle size of 38-45 μm contains a dominant quantity of monoclinic $Gd_5Ge_2Si_2$ -type phase and a small quantities of orthorhombic-I Gd_5Si_4 -type, orthorhombic-II Sm_5Ge_4 -type and hexagonal Mn_5Si_3 -type. The monoclinic $Gd_5Ge_2Si_2$ -type is responsible for GMCE [3]; the other phases are present because, probably, $Gd_{5.09}Ge_{2.03}Si_{1.88}$ is not a congruent melting composition.

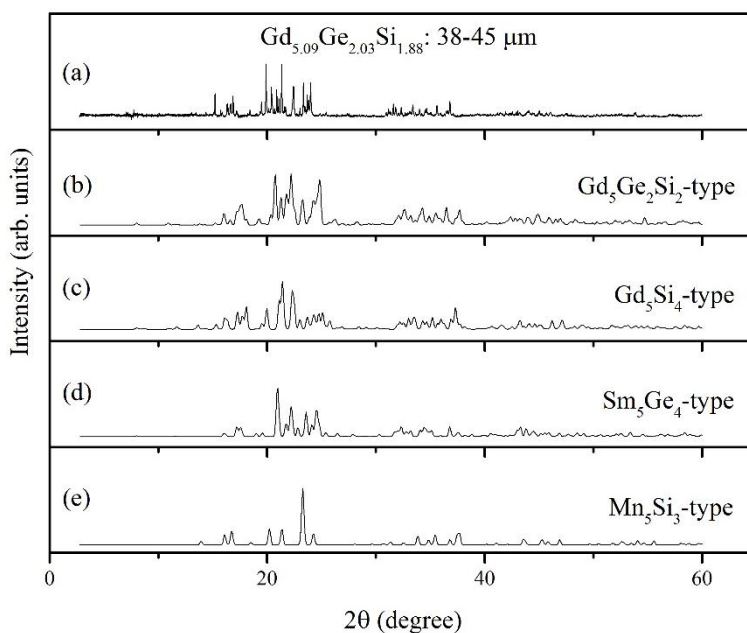


Fig. 1 – X-ray powder patterns of (a) $Gd_{5.09}Ge_{2.03}Si_{1.88}$ (38-45 μm) compared with (b) $Gd_5Ge_2Si_2$ -type (ICSD Coll Code 84084), (c) Gd_5Si_4 - (ICSD Coll Code 84083), (d) Sm_5Ge_4 - (ICSD Coll Code 84085), and (e) Mn_5Si_3 - (ICSD Coll Code 99641).

We note from magnetization as a function of temperature (M vs. T – Fig. 2a) data that our magnetocaloric base-powder $Gd_{5.09}Ge_{2.03}Si_{1.88}$ has a hysteretic first-order transition (~ 269 K on heating) and a small second-order transition (~ 306 K), similar to the $Gd_{5.09}Ge_{2.03}Si_{1.88}$ bulk

as-cast compound reported by Pires *et al.* [11]. During cooling cycle in the vicinity of the first-order transition, the base-powder undergoes a magnetostructural transition from paramagnetic (PM) monoclinic (M) to ferromagnetic (FM) orthorhombic-I (OI), *i.e.*, PM-M $\xrightarrow[1^{st} \text{ord. trans.}]{\text{cooling}}$ FM-OI, and vice-versa during heating cycle [4]. In the second-order transition, there is a purely magnetic transition from PM-OI to FM-OI during cooling cycle, *i.e.*, PM-OI $\xrightarrow[2^{nd} \text{ord. trans.}]{\text{cooling}}$ FM-OI, and vice-versa during heating cycle [4].

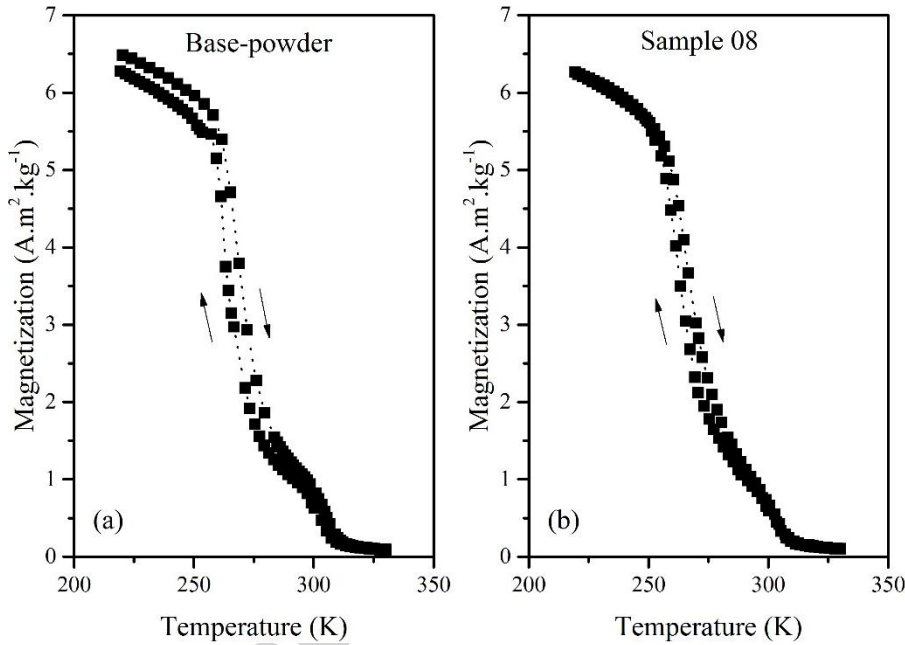


Fig. 2 – M vs. T curves at low field ($H=200$ Oe) of: (a) Base-powder: $\text{Gd}_{5.09}\text{Ge}_{2.03}\text{Si}_{1.88}$ with particle size of 38-45 μm ; and (b) Sample 08: 3 wt.% of PANi-CSA, sintering at 443 K for 5 h. The heating and cooling cycles are shown by rows.

Furthermore, the $|\Delta S_T^{pk}|$ from isothermal variation of entropy as a function of temperature ($-\Delta S_T$ vs. T in Fig. 3a) had a value of $\sim 8.1 \text{ J.kg}^{-1}.\text{K}^{-1}$ for a magnetic field variation of 20 kOe, smaller than the $\text{Gd}_5\text{Ge}_2\text{Si}_2$ proposed by Pecharsky and Gschneidner Jr. [3] ($\sim 14 \text{ J.kg}^{-1}.\text{K}^{-1}$), but proportional when compared to Pires *et al.* [11] ($\sim 14 \text{ J.kg}^{-1}.\text{K}^{-1}$ for

$\Delta H=0-50$ kOe). Transition temperature also occurred at ~ 269 K – as in references. [3,11] –, but with low purity Gd. Although, it was measured a δT_{FWHM} of ~ 15.7 K, providing a $RCP(S)$ of ~ 126.6 J.kg $^{-1}$.

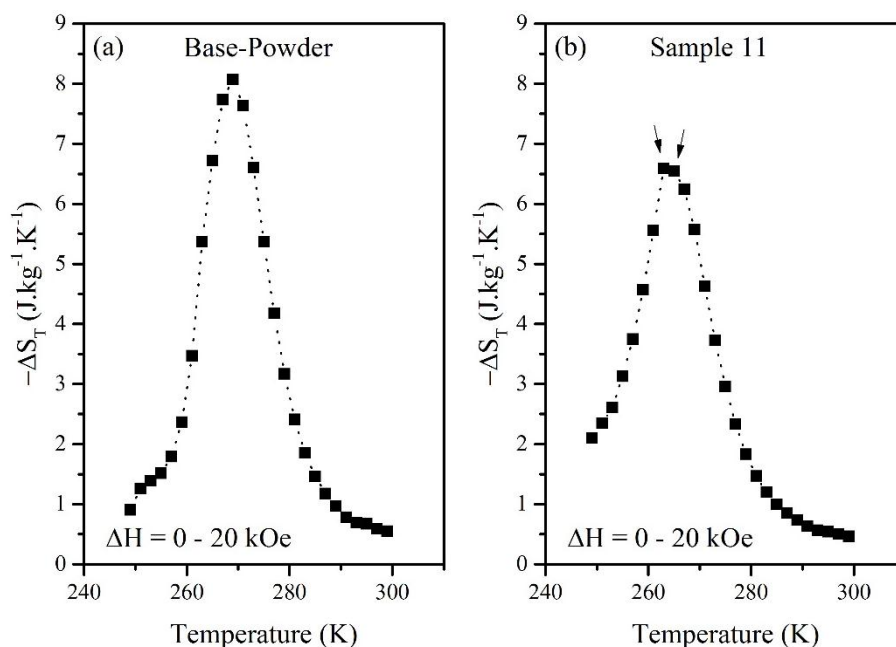


Fig. 3 – Isothermal variation of entropy (ΔS_T) at a magnetic field variation from 0 to 20 kOe for: (a) Base-powder: $Gd_{5.09}Ge_{2.03}Si_{1.88}$ with particle size of 38-45 μm ; and (b) Sample 11: 15 wt.% of PANi-CSA, sintering at 443 K for 5 h. The rows represent the ΔS_T almost parallel to temperature-axis near the first-order transition.

A SEM image of $Gd_{5.09}Ge_{2.03}Si_{1.88}$ with particle size of 38-45 μm is illustrated in Fig. 4. It was observed that the powder particles do not have a defined geometry and they are in the range of 38-45 μm . It is also noted that much smaller particles remained on the surface of the bigger particles due to electrostatic induction during the manual milling. The importance of ensures a particle size of 38-45 μm is justified in the fact that smaller sizes have smaller MCE, while much larger sizes do not present significant gain in MCE [21]; in other word, the particle size range of 38-45 μm is an ideal limit for making the PANi-CSA/ $Gd_{5.09}Ge_{2.03}Si_{1.88}$ composites.

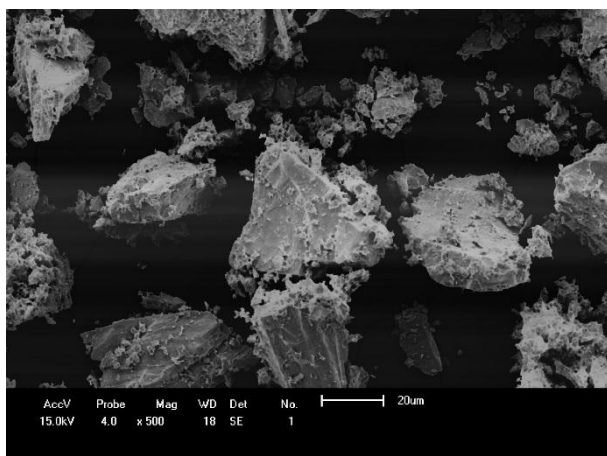


Fig. 4 – SEM image of $\text{Gd}_{5.09}\text{Ge}_{2.03}\text{Si}_{1.88}$ with particle size of 38-45 μm .

3.2. *PAni-CSA*

The XRD patterns of *PAni-CSA* (Fig. 5) show amorphous and crystalline characteristic. The sharp peak at $2\theta \sim 6.4^\circ$ is assigned to the periodic distance between the CSA and the N atom on adjacent main chains [22]. The most intense peak at $2\theta \sim 25^\circ$ is commented as a characteristic of the extent of conjugated π bonds in *PAni* [22]. The CSA also reflected in crystallinity of *PAni* ($2\theta \sim 8.7^\circ$, $\sim 15^\circ$, $\sim 20^\circ$ e $\sim 25^\circ$) not leaving it completely amorphous [23]. Moreover, the peaks at $2\theta \sim 15^\circ$ and $\sim 25^\circ$ can be attributed to remaining crystalline *PAni* without CSA, and $2\theta \sim 20^\circ$ to remaining nanocrystalline *PAni* without CSA [23].

The thermal stabilities of *PAni-CSA* is shown in TG (Fig. 6a) and DSC (Fig. 6b) diagrams. From TG diagram, we observe up to ~ 373 K a $\sim 10\%$ weight loss due to water and oligomers, and between ~ 373 and ~ 500 K, $\sim 5\%$ weight loss is due to loss of solvent from the amorphous phase [24]. Thereafter, above ~ 500 K occurs the degradation of CSA, and then degradation of *PAni* [24]. Endothermic peaks at ~ 373 and ~ 525 K are confirmed by DSC diagram too, and they are important to guarantee non-degradation of *PAni-CSA* during the sintering at 443 K for 5 h.

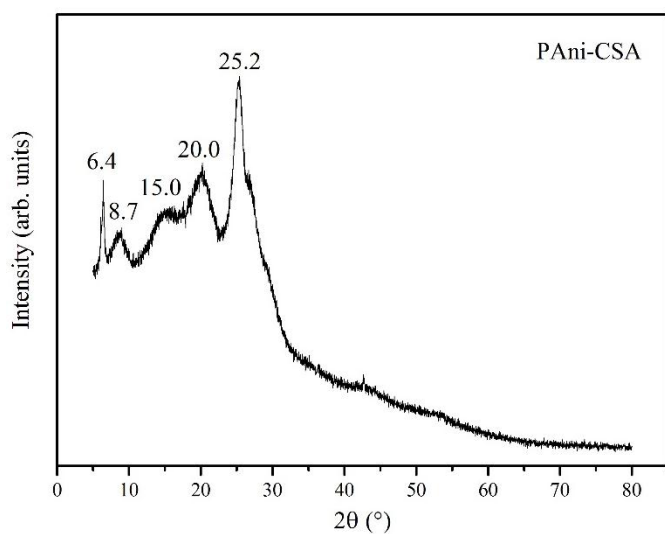


Fig. 5 – X-ray powder patterns of PANi-CSA.

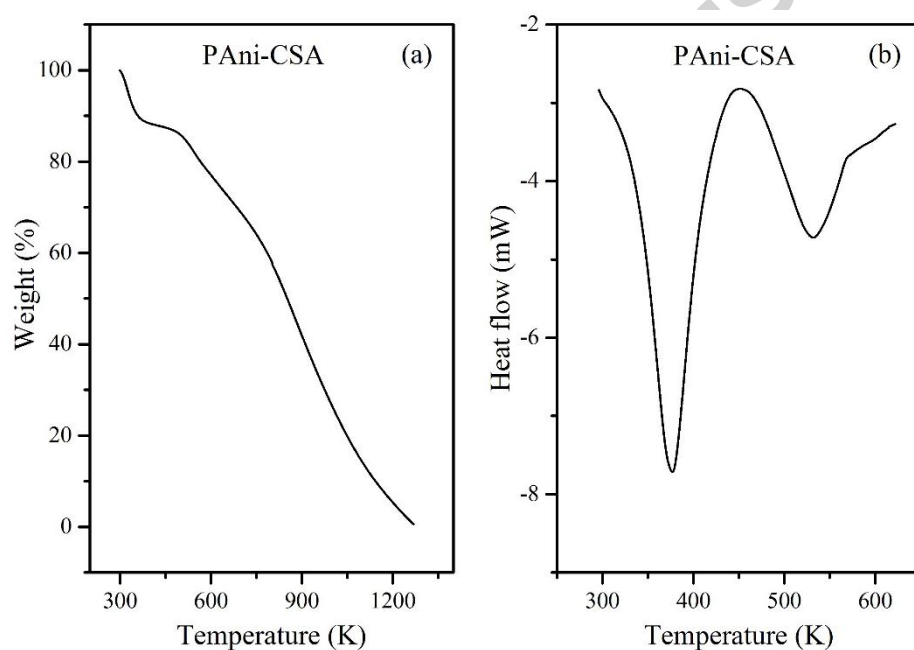


Fig. 6 – (a) TG diagram of PANi-CSA; and (b) DSC diagram of PANi-CSA.

The oxidation state and protonation of PANi-CSA were observed in FTIR spectrum (Fig. 7a). The bands at 1558 and 1480 cm^{-1} are associated with the C=C stretching and C–H bending deformation of semiquinone emeraldine base, respectively, due to oxidation of PANi

[25,26,27], in addition to C-C stretching of quinoid (Q) and benzenoid rings (B), respectively [28]. The band at 1300 cm^{-1} is assigned to the C-N stretching of secondary (-N=) aromatic amine group for B or π electron delocalization induced in PANi by CSA [22,23]. The peak at 1243 cm^{-1} is related to the C-N^+ or C=N^+ stretching vibration in the polaron structure due to PANi doped by CSA [27,28]. The bands at 1103 , 696 e 616 cm^{-1} have identified the sulfonate SO_3^- groups attached to B [26]. The band at 588 and 880 cm^{-1} is due to C-C stretching of B and C-H bending out-of-plane on Q [29]. Finally, the peak 803 cm^{-1} is associated with stretching of SO_3^- groups and C-H bending out-of-plane on B [28].

The UV-Vis spectrum of PANi-CSA is illustrated in Fig. 7b and show three distinctive peaks. The peak at *ca.* 330 nm is related to the $\pi - \pi^*$ transition of B, the peak at *ca.* 450 nm is assigned for polaron- π^* , and the peak at *ca.* 630 nm is due to $n-\pi$ transition of Q [30]. From the EIS data, the electrical conductivity (σ) was evaluate in $(1.20 \pm 0.43) \times 10^{-3}\text{ S.m}^{-1}$.

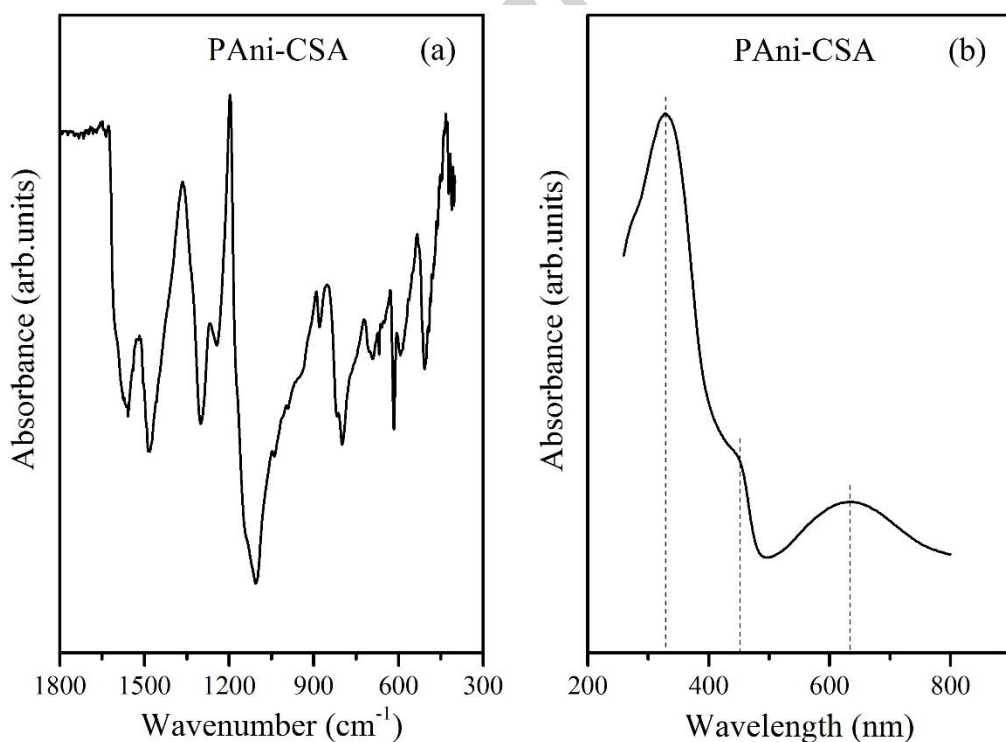


Fig. 7 – (a) FTIR spectrum of PANi-CSA, and (b) UV-Vis spectrum of PANi-CSA

3.3. *PAni-CSA/Gd_{5.09}Ge_{2.03}Si_{1.88}*

The sintering at 443 K for 5 h tended to increase the Vickers hardness values when compared with samples that have same concentration of PAni-CSA but non-sintering (Fig. 8). This was expected due to the coalescence of PAni-CSA particles, because the temperature of 443 K is not sufficient to degrade CSA and polymer chains as shown in TG (Fig. 6a) and DSC (Fig. 6b) diagrams of PAni-CSA. The minimum point that occurs at 9 wt.% is probably arising from the difference between the density of PAni-CSA and $Gd_{5.09}Ge_{2.03}Si_{1.88}$, and how these parts interact with each other.

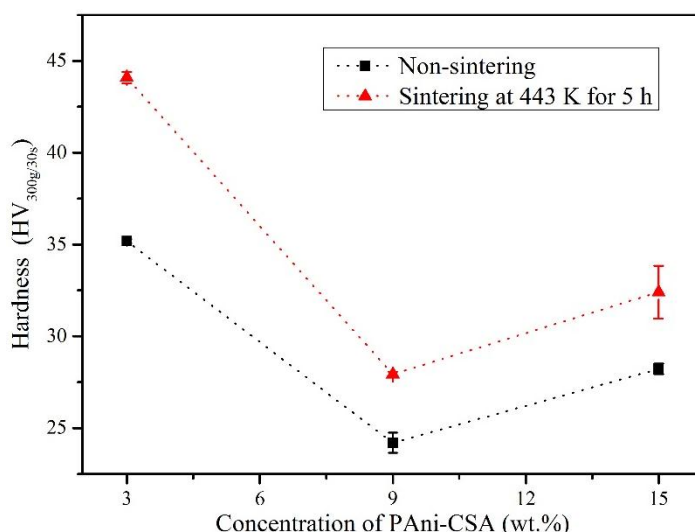


Fig. 8 – Vickers hardness *vs.* concentration of PAni-CSA in $PAni-CSA/Gd_{5.09}Ge_{2.03}Si_{1.88}$ composites.

This interaction can be understood by SEM images (Fig. 9). $Gd_{5.09}Ge_{2.03}Si_{1.88}$ powders arrange during the compaction while PAni-CSA acts absorbing the load, leaving the particles intact. Higher magnifications of SEM (not shown here) prove that the magnetocaloric reinforcement has the same particle size as before compaction process. Moreover, the interior has a porous and irregular aspect, but it is due to intergranular fracture (*i.e.*, these pseudo-

porous are vacancies of particles that were there before being pulled). Although all PANi-CSA/Gd_{5.09}Ge_{2.03}Si_{1.88} composites can be handled without fracturing, we observed that low concentrations of PANi-CSA give more fragile characteristic (see some cracks in Fig. 9a-b), while high concentrations give more ductile characteristic (see in Fig. 9d the artifact whose geometry is a linear risk with well-defined depth which was derived from the blade used in fracture process). It was interesting to realize how increasing concentration of PANi-CSA made more and more difficult to fracture the samples, and how two samples with the same concentration – but sometimes sintered, sometimes not – also had more difficulty to fracture when the PANi-CSA/Gd_{5.09}Ge_{2.03}Si_{1.88} composite was sintered.

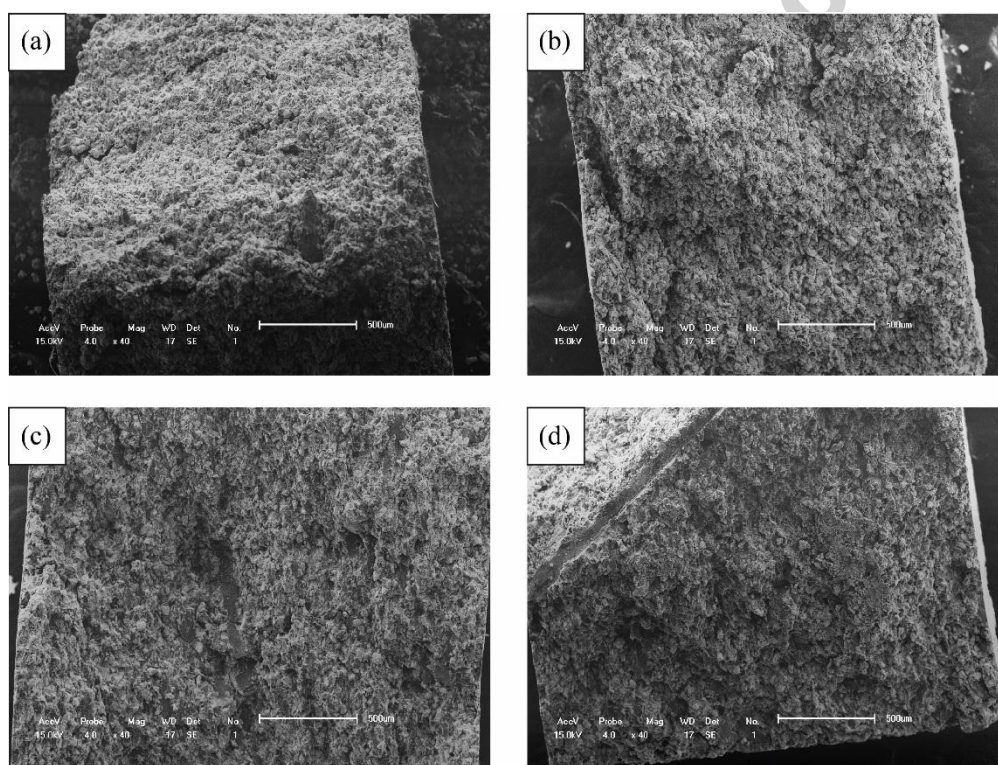


Fig. 9 – SEM images of PANi-CSA/Gd_{5.09}Ge_{2.03}Si_{1.88} composites: (a) 3 wt.% of PANi-CSA, non-sintering; (b) 3 wt.% of PANi-CSA, sintering at 443 K for 5 h; (c) 15 wt.% of PANi-CSA, non-sintering; and (d) 15 wt.% of PANi-CSA, sintering at 443 K for 5 h.

As all PAni-CSA/Gd_{5.09}Ge_{2.03}Si_{1.88} composites had 0.200 g, we can measure the height (Fig. 10) to evaluate the difference between the density of PAni-CSA and Gd_{5.09}Ge_{2.03}Si_{1.88}, and the influence of sintering. The height tended to increase with increasing the concentration of PAni-CSA because Gd_{5.09}Ge_{2.03}Si_{1.88} is much denser than PAni-CSA, while sintering contributed to reduce the height due to the coalescence of PAni-CSA particles, analogous to what happens with metal or ceramic pieces produced by powder metallurgy.

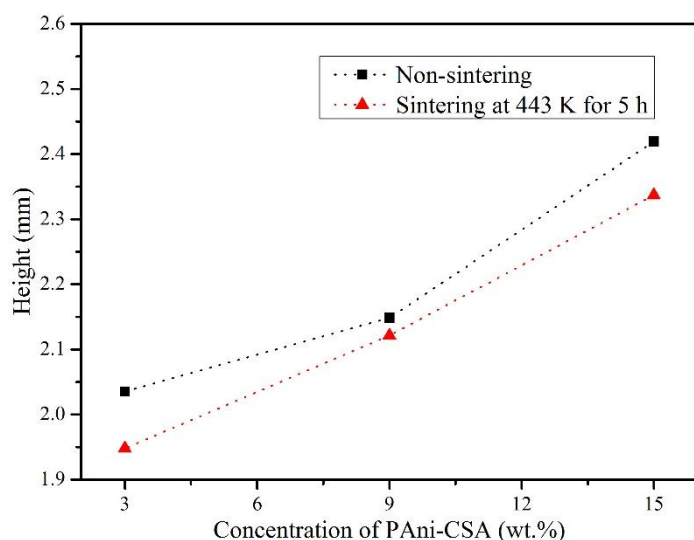


Fig. 10 – Height *vs.* concentration of PAni-CSA in PAni-CSA/Gd_{5.09}Ge_{2.03}Si_{1.88} composites.

From magnetization as a function of temperature (*M vs. T*) data, all PAni-CSA/Gd_{5.09}Ge_{2.03}Si_{1.88} has a hysteretic first-order transition and a second-order transition (see an example in Fig. 2b and all the results in Table 1). Notwithstanding, the first- and a second-order seem different among the composites; this can be partially explained by the relatively low precision in the determination of local minima in *dM/dT vs. T* curves, mainly around the second-order transitions (not shown). On the other hand, we can take average values and show that samples was sintered at 443 K for 5 h present a first-order transition at ~ 265 K on

heating and a second-order transition at ~ 304 K, while non-sintered samples present first- and second-order transition at ~ 267 and ~ 303 K, respectively. Comparing this to our magnetocaloric base-powder $\text{Gd}_{5.09}\text{Ge}_{2.03}\text{Si}_{1.88}$ from section 3.1, we can say that compact process decrease the first- and second-order transition by ~ 2 and ~ 3 K, respectively, and the sintering process decrease the first-order transition more ~ 2 K.

From $-\Delta S_T$ as a function of temperature curves (not shown here, only an example in Fig. 3b), we also calculated the temperature of the peak (T^{pk}), $|\Delta S_T^{pk}|$ and $RCP(S)$ of PANi-CSA/ $\text{Gd}_{5.09}\text{Ge}_{2.03}\text{Si}_{1.88}$ composites as follow in Table 1.

Table 1 – Magnetic and magnetocaloric properties of PANi-CSA/ $\text{Gd}_{5.09}\text{Ge}_{2.03}\text{Si}_{1.88}$ composites and $\text{Gd}_{5.09}\text{Ge}_{2.03}\text{Si}_{1.88}$ base-powder.

	Factors		Properties				
	A	B	1 st trans.	2 nd trans.	T^{pk}	$ \Delta S_T^{pk} $	$RCP(S)$
Samples	PAni-CSA (wt.%)	Sintering (443 K for 5 h)	heating cooling (K K)	heating cooling (K K)	(K)	(K)	(J.kg ⁻¹)
01	3	No	267 261	301 301	267	7.7	133.2
02	3	No	269 263	305 299	267	7.0	119.4
03	9	No	267 261	302 301	267	7.1	122.9
04	9	No	269 261	305 303	267	6.1	103.3
05	15	No	267 259	304 301	267	5.7	99.40
06	15	No	267 261	305 299	267	5.9	101.0
07	3	Yes	267 261	305 299	265	7.8	131.5
08	3	Yes	265 261	303 299	265	7.3	124.4
09	9	Yes	265 261	303 301	265	6.4	111.6
10	9	Yes	267 259	304 303	265	8.0	137.7
11	15	Yes	265 261	305 301	263	6.6	122.6

Factors			Properties				
	A	B	1 st trans.	2 nd trans.	T^{pk}	$ \Delta S_T^{pk} $	$RCP(S)$
Samples	PAni-CSA (wt.%)	Sintering (443 K for 5 h)	heating cooling (K K)	heating cooling (K K)	(K)	(K)	(J.kg ⁻¹)
12	15	Yes	265 257	306 299	263	5.7	101.2
Base- powder	-	-	269 263	306 306	269	8.1	126.6

Sintering at 443 K for 5 h tended to decrease T^{pk} , but it is not affected by the concentration of PAni-CSA. Even though the 15 wt.% sintered composites had T^{pk} at 263 K, this reduction of 2 K when compared to others sintered samples ($T^{pk} \sim 265$ K) can be explained, because the sintered composites usually present a table-like peak with ΔS really close to $|\Delta S_T^{pk}|$ at slightly above temperature (*i.e.*, the vicinity of $|\Delta S_T^{pk}|$ is almost parallel to temperature-axis; see an example in Fig. 3b). The $|\Delta S_T^{pk}|$ (Fig. 11a) and the $RCP(S)$ (Fig. 11b) are inversely proportional to the concentration of PAni-CSA due to its non-magnetic contribution. The influence of sintering on $|\Delta S_T^{pk}|$ and $RCP(S)$ was difficult to evaluate owing to some inconstancy in duplicates.

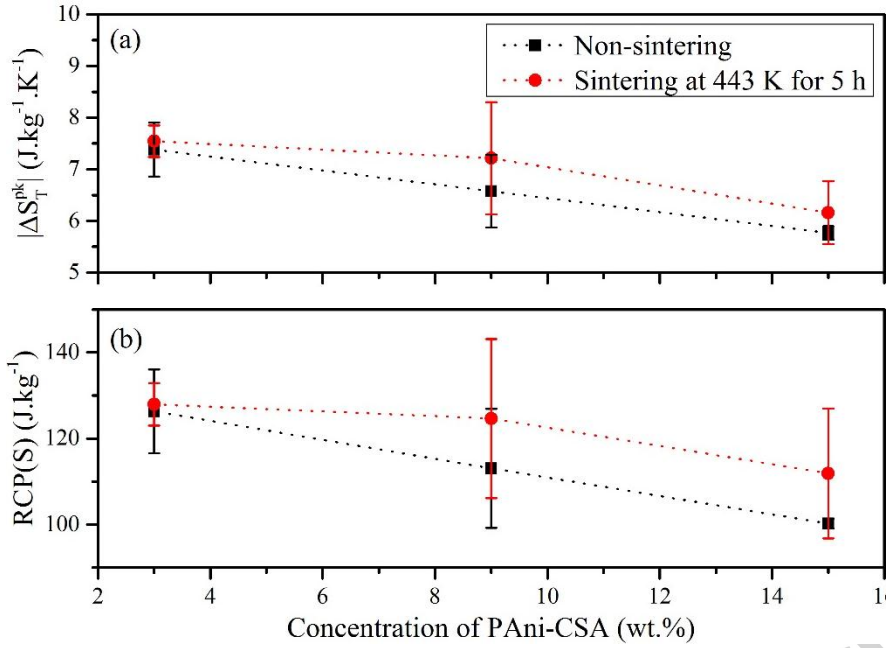


Fig. 11 – (a) Peak of isothermal variation of entropy ($|\Delta S_T^{pk}|$) *vs.* concentration of PANi-CSA in PANi-CSA/Gd_{5.09}Ge_{2.03}Si_{1.88} composites; and (b) Relative cooling power ($RCP(S)$) *vs.* concentration of PANi-CSA in PANi-CSA/Gd_{5.09}Ge_{2.03}Si_{1.88} composites.

The difference in the composites with same composition and process is probably due to the manually compacting process. Compacting granular materials – especially cases that use uniaxial pressure – must controls the displacement of the powder particles, their accommodation and the pressure gradient develop inside the pellet. In this paper, the controlled parameters (with confidence) were: the final pressure (250 MPa) measured in the sensor display and the pressure relief time (30 s). Thereby, the displacement of the powder particles, their accommodation and the pressure gradient probably presented variations among the samples, resulting in duplicates with small differences in their physical properties.

Of course, the manufacturing process of PANi-CSA/Gd_{5.09}Ge_{2.03}Si_{1.88} composites must control these variations for any applicability in magnetic refrigeration, but knowing that there is possibility to combine mechanical, electrical and magnetocaloric properties in this new composite give us a direction. Besides that, other magnetocaloric reinforcements can be used

(*e.g.*, La(Fe,Si)_{13} , MnAs) with different conductive polymers (*e.g.*, polypyrrole, polyacetylene).

4. Conclusions

We showed a new type of magnetocaloric composite based on conductive polymer and magnetocaloric compound. The $\text{PAni-CSA/Gd}_{5.09}\text{Ge}_{2.03}\text{Si}_{1.88}$ composites with low concentration of PAni-CSA (maximum of 15 wt.%) exhibited a drastic improvement on mechanical properties, while the worst result of *RCP* (sample 05) corresponded to a reduction of ~22% compared to the base-powder's *RCP*. All composites underwent a first- and second-order transition, consonant to the base-powder, showing that the compact process and the sintering had little influence on destroying the MCE. In short, because of different characteristics in conductive polymer matrix and magnetocaloric reinforcement, the $\text{PAni-CSA/Gd}_{5.09}\text{Ge}_{2.03}\text{Si}_{1.88}$ composite combines mechanical, electrical and magnetocaloric properties interesting to magnetic refrigeration technologies.

Acknowledgement

The authors acknowledge CAPES and CNPq for financial support.

References

- [1] A.M. Tishin, Y.I. Spichkin, Recent progress in magnetocaloric effect: Mechanisms and potential applications, *Int. J. Refrigeration* 37 (2014) 223-229.
- [2] C.S. Alves, F.C. Colman, G.L. Foleiss, W. Szpak, G.T.F. Vieira, A.C. Bento, Simulation of solar Curie wheel using NiFe alloy and Gd, *Int. J. Refrigeration* 37 (2014) 215-222.

- [3] V.K. Pecharsky, K.A. Gschneidner Jr., Giant Magnetocaloric Effect in $\text{Gd}_5\text{Si}_2\text{Ge}_2$, *Phys. Rev. Lett.* 78 (1997) 4494-4497.
- [4] A.O. Pecharsky, K.A. Gschneidner Jr, V.K. Pecharsky, The giant magnetocaloric effect of optimally prepared $\text{Gd}_5\text{Si}_2\text{Ge}_2$, *J. Appl. Phys.* 93 (2003) 4722-4728.
- [5] K.A. Gschneidner Jr, V.K. Pecharsky, Magnetic refrigeration materials (invited), *J. Appl. Phys.* 85 (1999) 5365-5368.
- [6] C.S. Alves, C.C. Colucci, S. Gama, A.M.G. Carvalho, A.A. Coelho, Influence of hydrogen on the magnetic behaviour of $\text{Gd}_5\text{Ge}_2\text{Si}_2\text{H}_x$, $0.1 \leq x \leq 2.5$, *J. Magn. Magn. Mater.* 272-276 (2004) 2391-2392.
- [7] A. Yan, A. Handstein, P. Kersch, K. Nenkov, K.-H. Müller, O. Gutfleisch, Effect of composition and cooling rate on the structure and magnetic entropy change in $\text{Gd}_5\text{Si}_x\text{Ge}_{4-x}$, *J. Appl. Phys.* 95 (2004) 7064-7066.
- [8] C. Magen, L. Morellon, P.A. Algarabel, M.R. Ibarra, Z. Arnold, J. Kamarad, T.A. Lograsso, D.L. Schlagel, V.K. Pecharsky, A.O. Tsokol, K.A. Gschneidner Jr, Hydrostatic pressure control of the magnetostructural phase transition in $\text{Gd}_5\text{Si}_2\text{Ge}_2$ single crystals, *Phys. Rev. B* 72 (2005) 024416(1-7).
- [9] G.G. Couto, V. Svitlyk, M. Jafelicci Jr., Y. Mozharivskyj, Bulk and high-energy ball-milled $\text{Gd}_5\text{Si}_2\text{Ge}_2$: Comparative study of magnetic and magnetocaloric properties, *Solid State Sci.* 13 (2011) 209-215.
- [10] S. Gama, C.S. Alves, A.A. Coelho, C.A. Ribeiro, A.I C. Persiano, D. Silva, On the determination of the phase composition of the $\text{Gd}_5\text{Ge}_2\text{Si}_2$ alloy, *J. Magn. Magn. Mater.* 272-276 (2004) 848-849.

- [11] M.J.M. Pires, A.M.G. Carvalho, S. Gama, E.C. da Silva, A.A. Coelho, A.M. Mansanares, Electron spin resonance and magnetic characterization of the $\text{Gd}_{5.09}\text{Ge}_{2.03}\text{Si}_{1.88}$, *Phys. Rev. B* 72 (2005) 224435(1-5).
- [12] K.P. Skokov, D.Y. Karpenkov, M.D. Kuz'min, I.A. Radulov, T. Gottschall, B. Kaeswurm, M. Fries, O. Gutfleisch, Heat exchangers made of polymer-bonded $\text{La}(\text{Fe},\text{Si})_{13}$, *J. Appl. Phys.* 115 (2014) 17A941(1-3).
- [13] H. Zhang, Y. Sun, E. Niu, F. Hu, J. Sun, B. Shen, Enhanced mechanical properties and large magnetocaloric effects in bonded $\text{La}(\text{Fe},\text{Si})_{13}$ -based magnetic refrigeration materials, *Appl. Phys. Lett.* 104 (2014) 062407(1-4).
- [14] H. Zhang, Y. Sun, Y. Li, Y. Wu, Y. Long, J. Shen, F. Hu, J. Sun, B. Shen, Mechanical properties and magnetocaloric effects in $\text{La}(\text{Fe}, \text{Si})_{13}$ hydrides bonded with different epoxy resins, *J. Appl. Phys.* 117 (2015) 063902(1-4).
- [15] B. Pulko, J. Tušek, J.D. Moore, B. Weise, K. Skokov, O. Mityashkin, A. Kitanovski, C. Favero, P. Fajfar, O. Gutfleisch, A. Waske, A. Poredoš, Epoxy-bonded La-Fe-Co-Si magnetocaloric plates, *J. Magn. Magn. Mater.* (2015) 65-73.
- [16] J. Lanzarini, T. Barriere, M. Sahli, J.C. Gelin, A. Dubrez, C. Mayer, M. Pierronnet, P. Vikner, Thermoplastic filled with magnetocaloric powder, *Mater. Des.* 87 (2015) 1022-1029.
- [17] H. Canova, A. Fontoura, R.T. Neuenschwander, B. Dias, C.B. Rodella, Upgrades to the XRD1 beamline optics and endstation at the LNLS, *JPCS* 493 (2014) 012004(1-4).
- [18] V.K. Pecharsky, K.A. Gschneidner Jr., Magnetocaloric effect from indirect measurements: Magnetization and heat capacity, *J. Appl. Phys.* 86 (1999) 565-575.
- [19] K.A. Gschneidner Jr, V.K. Pecharsky, Magnetocaloric materials, *Annu. Rev. Mater. Sci.* 30 (2000) 387-429.

- [20] E.M. Giroto, M.A de Paoli, Transporte de massa em polímeros intrinsecamente condutores: Impedância, técnicas e modelos teóricos, *Quim. Nova* 22 (1999) 358-368.
- [21] GEMMA-UEM (Magnetocaloric Materials Studies Group of State University of Maringá), unpublished information.
- [22] M. Amrithesh, S. Aravind, S. Jayalekshmi, R.S. Jayasree, Polyaniline doped with orthophosphoric acid – A material with prospects for optoelectronic applications, *J. Alloy Compd.* 458 (2008) 532-535.
- [23] S.A. Chen, H.T. Lee, Polyaniline plasticized with 1-methyl-2-pyrrolidone: Structure and doping behavior, *Macromolecules* 26 (1993) 3254-3261.
- [24] L. Abell, S.J. Pomfret, P.N. Adams and A.P. Monkman, Thermal studies of doped polyaniline, *Synt. Met.* 84 (1997) 127-128.
- [25] M.-I. Boyer, S. Quillard, E. Rebourt, G. Louarn, J. P. Buisson, A. Monkman, S. Lefrant, Vibrational analysis of polyaniline: A model compound approach, *J. Phys. Chem. B* 102 (1998) 7382-7392.
- [26] M. Trchová, I. Šeděnková, E.N. Konyushenko, J. Stejskal, P. Holler, G. Ćirić-Marjanović, Evolution of polyaniline nanotubes: The oxidation of aniline in water, *J. Phys. Chem. B* 110 (2006) 9461-9468.
- [27] M.C. Arenas, G. Sánchez, M.E. Nicho, J. Elizalde-Torres, V.M. Castaño, Engineered doped and codoped polyaniline gas sensors synthesized in N,N-dimethylformamide media, *Appl. Phys. A* 106 (2012) 901-908.
- [28] V.J. Babu, S. Vempati, S. Ramakrishna, Conducting polyaniline-electrical charge transportation *Mater. Sci. Appl.* 4 (2013) 1-10.
- [29] M.Trchová, J. Stejskal, J. Prokeš, Infrared spectroscopic study of solid-state protonation and oxidation of polyaniline, *Synt. Met.* 101 (1999) 840-841.

[30] O. Abdulrazzaq, S.E. Bourdo, V. Saini, F. Watanabe, B. Barnes, A. Ghoshb, A.S. Birisa, Tuning the work function of polyaniline via camphorsulfonic acid: An X-ray photoelectron spectroscopy investigation RSC Adv. 5 (2015) 33-40.

Fig. 1 – X-ray powder patterns of (a) $\text{Gd}_{5.09}\text{Ge}_{2.03}\text{Si}_{1.88}$ (38-45 μm) compared with (b) $\text{Gd}_5\text{Ge}_2\text{Si}_2$ -type (ICSD Coll Code 84084), (c) Gd_5Si_4 - (ICSD Coll Code 84083), (d) Sm_5Ge_4 - (ICSD Coll Code 84085), and (e) Mn_5Si_3 - (ICSD Coll Code 99641).

Fig. 2 – M vs. T curves at low field ($H=200$ Oe) of: (a) Base-powder: $\text{Gd}_{5.09}\text{Ge}_{2.03}\text{Si}_{1.88}$ with particle size of 38-45 μm ; and (b) Sample 08: 3 wt.% of PANi-CSA, sintering at 443 K for 5 h. The heating and cooling cycles are shown by rows.

Fig. 3 – Isothermal variation of entropy (ΔS_T) at a magnetic field variation from 0 to 20 kOe for: (a) Base-powder: $\text{Gd}_{5.09}\text{Ge}_{2.03}\text{Si}_{1.88}$ with particle size of 38-45 μm ; and (b) Sample 11: 15 wt.% of PANi-CSA, sintering at 443 K for 5 h. The rows represent the ΔS_T almost parallel to temperature-axis near the first-order transition.

Fig. 4 – SEM image of $\text{Gd}_{5.09}\text{Ge}_{2.03}\text{Si}_{1.88}$ with particle size of 38-45 μm .

Fig. 5 – X-ray powder patterns of PANi-CSA.

Fig. 6 – (a) TG diagram of PANi-CSA; and (b) DSC diagram of PANi-CSA.

Fig. 7 – (a) FTIR spectrum of PANi-CSA, and (b) UV-Vis spectrum of PANi-CSA

Fig. 8 – Vickers hardness vs. concentration of PANi-CSA in PANi-CSA/ $\text{Gd}_{5.09}\text{Ge}_{2.03}\text{Si}_{1.88}$ composites.

Fig. 9 – SEM images of PANi-CSA/ $\text{Gd}_{5.09}\text{Ge}_{2.03}\text{Si}_{1.88}$ composites: (a) 3 wt.% of PANi-CSA, non-sintering; (b) 3 wt.% of PANi-CSA, sintering at 443 K for 5 h; (c) 15 wt.% of PANi-CSA, non-sintering; and (d) 15 wt.% of PANi-CSA, sintering at 443 K for 5 h.

Fig. 10 – Height vs. concentration of PANi-CSA in PANi-CSA/ $\text{Gd}_{5.09}\text{Ge}_{2.03}\text{Si}_{1.88}$ composites.

Fig. 11 – (a) Peak of isothermal variation of entropy ($|\Delta S_T^{pk}|$) vs. concentration of PAni-CSA in PAni-CSA/Gd_{5.09}Ge_{2.03}Si_{1.88} composites; and (b) Relative cooling power (RCP(S)) vs. concentration of PAni-CSA in PAni-CSA/Gd_{5.09}Ge_{2.03}Si_{1.88} composites.

Highlights:

1. We developed a new type of magnetocaloric composite: PAni-CSA/Gd_{5.09}Ge_{2.03}Si_{1.88};
2. We presented a processing route which use a conductive polymer instead of epoxy resins or thermoplastic polymers;
3. We varied the concentration of PAni-CSA (numerical type) and sintering (categorical type);
4. We analyzed the matrix (PAni-CSA), the magnetocaloric reinforcement (Gd_{5.09}Ge_{2.03}Si_{1.88}) and the composites;
5. We presented and discussed mechanical, electrical and magnetocaloric properties.